IEEE Photonics Journal
An IEEE Photonics Society Publication

Photon-Counting Underwater Wireless Optical Communication by Recovering Clock and Data From Discrete Single Photon Pulses

Volume 11, Number 5, October 2019

Qiurong Yan
Zihang Li
Zhu Hong
Ting Zhan
Yuhao Wang

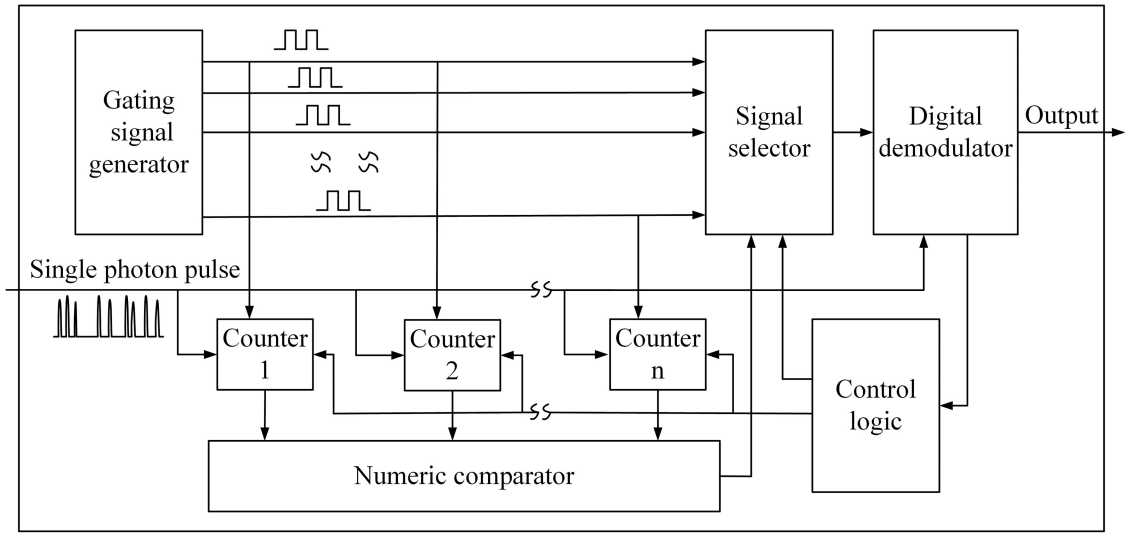

DOI: 10.1109/JPHOT.2019.2936833

Photon-Counting Underwater Wireless Optical Communication by Recovering Clock and Data From Discrete Single Photon Pulses

Qiurong Yan, Zihang Li, Zhu Hong, Ting Zhan, and Yuhao Wang

Department of Electronics Information Engineering, Nanchang University, Nanchang 330031, China

DOI:10.1109/JPHOT.2019.2936833

Manuscript received July 20, 2019; revised August 14, 2019; accepted August 18, 2019. Date of publication August 22, 2019; date of current version September 5, 2019. This work was supported in part by the National Natural Science Foundation of China under Grants 61865010 and 61565012, in part by the China Postdoctoral Science Foundation under Grant 2015T80691, in part by the Science and Technology Plan Project of Jiangxi Province under Grant 20151BBE50092, and in part by the Funding Scheme to Outstanding Young Talents of Jiangxi Province under Grant 20171BCB23007. Corresponding author: Qiurong Yan (e-mail: yanqiurong@ncu.edu.cn).

Abstract: To realize a long-distance underwater communication by using low-cost light emitting diode (LED) and single photon avalanche diode (SPAD), we proposed a method for recovering clock and data directly from discrete random pulse sequences output by SPAD. On this basis, a new communication model is established, taking into account not only fluctuations in photon flux and quantum efficiency of photon detection in a time-slot, but also the phase difference of the recovered clock caused by it. A photon-counting underwater optical wireless communication (UOWC) system was built. The effects of the system setting parameters such as the number of gating signals, synchronous character length and baud rate on the average bit error rate (BER) were verified by experiments. The experimental results show that under condition of only average 10 photons in one time-slot, photon-counting UOWC with a BER of 3.51×10^{-4} and a baud rate of 1 Mbps can be achieved.

Index Terms: Underwater optical wireless communication (UOWC), photon-counting, clock synchronization, data recovery.

1. Introduction

Underwater wireless communication has attracted more and more attention and plays an important role in military, environmental detection, offshore exploration and disaster prevention [1]–[4]. At present, there are communication technologies such as ultrasound, radio frequency (RF) and optics for underwater data transmission. Ultrasonic communication can achieve long-distance communication over kilometers, but the communication rate is very low (Kbps) due to the problems of high latency, multipath propagation and doppler shift. Although the RF can realize high-speed communication, the electromagnetic wave is limited to achieving short-distance transmission because of the serious attenuation underwater. Since the optical window of blue-green band (430–520 nm) has less attenuation underwater, the underwater optical wireless communication (UOWC) in the blue-green band stands as the best option for underwater high-speed communications in medium and long distance. Besides, it has the advantages of small size, low power consumption and high security.

At the transmitting terminal of wireless optical communication, a laser diode (LD) or light emitting diode (LED) is used to emit optical signal [5]–[9]. With the advantages of low cost, convenient alignment and high power, LED-based visible light communication technology is increasingly adopted in underwater wireless communication devices [10]–[15]. Compared to LD, LED has a large emission angle, which results in severe geometric attenuation and short communication distance. At the receiving terminal of traditional wireless optical communication systems, PIN photodiode and avalanche photo diode (APD) detectors are mostly used to detect optical signal [16]–[20]. The detector works in the analog mode, the photocurrent signal output by detector is amplified by a transimpedance amplifier (TIA), and the receiving terminal demodulates the communication signal from the amplified current signal. The low noise design of the TIA is the key to improve detection sensitivity and communication distance.

In recent years, single photon detectors with single photon sensitivity were used to detect the optical signal at the receiving terminal, and good results have been achieved in deep space laser communication, atmospheric laser communication, indoor visible light communication and other fields [21]–[33]. With the increasing demand for various underwater vehicles, sensors and obvservation, using the low-cost LED and single photon detector to realize long-distance underwater communication has become a research hotspot. In 2014, Philip A. *et al.* developed a photon-counting wireless optical communication system for underwater data transmission using single photon avalanche diode (SPAD) [34]. A long distance underwater visible light communication based on a SPAD receiver is designed and a two-term exponential channel model is established in [22]. Multiple LED chips parallel transmission scheme for underwater visible light communication system with one photon-counting SPAD receiver is proposed in [7]. The use of Silicon photo-multipliers (SiPM) for underwater wireless communication is studied in [27]. A photon-counting receiver system for long-distance underwater wireless laser communication at different code rate Reed-Solomon (RS) and low-density parity check (LDPC) codes is reported in [21]. A UOWC system based on single LED as well as a lens-free multi-pixel photon counter (MPPC) is proposed in [35]. After receiving the very weak light signal attenuated by the channel, the single photon detector outputs discrete random pulse sequences due to fluctuations in photon flux and quantum efficiency of photon detection. Most of these pulses represent detected signal photons but also include a few of noise pulses caused by background photons and dark count. In the above literature, how to demodulate transmission information from these discrete random pulses is not described in detail and completely. A relatively simple way is to demodulate the optical signal in analog mode after the random pulses from the single photon detector pass through a filter. This method only takes advantage of the high gain of the single photon detector, and the communication rate will be limited by filter bandwidth. Demodulation of communication signals includes clock and data recovery, where clock recovery is the basis for data recovery. The recovered clock includes three levels of synchronous clocks of time-slot, symbol and frame, where the recovery of the time-slot clock is the basis of the other two levels. Time-slot is the smallest unit of information transmission. Multiple time-slots constitute a symbol, and multiple symbols constitute a frame. Therefore, how to recover the time-slot synchronization clock from the discrete random single photon pulse is the key to the demodulation of the photon counting communication signal.

In order to realize a long-distance UOWC, we propose and implement a method for directly recovering clock and data from discrete random pulse sequence output by SPAD. Based on this method, a communication model is established, and a long-distance photon-counting UOWC experimental system for verification is bulit.

2. System Model

2.1 LED Emission Light Field and Underwater Channel Attenuation

In the photon-counting wireless optical communication system, the optical signal should be regarded as discrete photon stream. Due to the bunching effect of photons, the photon stream generated by LED is Poisson distribution rather than Uniform distribution. We assume that the average number

TABLE 1
Parameters of the SPAD and the Optics System

Part number	SPCM20A
Wavelength range	350-900 nm
Active detector size	Ø20 μm
Max efficiency	35%@500 nm
Dark count rate	25 Hz
Max count rate	28 MHZ
Deadtime	40 ns
Pulse width	20 ns
L	1.5 m

of photons in each time-slot is μ. Then, the probability that the LED emits n photons in each symbol can be expressed as

$$P(n, \mu) = \frac{\mu^n}{n!} \exp(-\mu) \tag{1}$$

Where $\mu = P_s T_s / E_1$, P_s denotes the LED optical power, T_s denotes length of time-slot, and E_1 denotes the energy of one photon.

In the pure seawater environment, we used Beer Law to describe the attenuation characteristics of optical signals under water. The power of the optical signal at the receiving terminal is $P_r(L) = P_s e^{-c(\lambda)L}$, where $c(\lambda)$ denotes the total attenuation coefficient in underwater channel, and L is the communication distance [36], [37]. Therefore, when $n = \mu$, the number of photons output by the SPAD can be expressed as

$$\lambda_{s[k]} = \frac{C_{PDE} P_s T_s}{E_1} \exp(-c(\lambda)L) + N_b = n C_{PDE} \exp(-c(\lambda)L) + N_b \tag{2}$$

Where C_{PDE} is the quantum efficiency of SPAD, N_b is the noise photons per time-slot, $s[k] \in \{0, 1\}$ is the transmitted NRZ-OOK symbol.

2.2 Time-Slot Synchronization

After the SPAD detects a photon, it takes some time to recover the ability to detect the next photon. This phenomenon, called dead time effect, results in that the statistical distribution of photons output by the SPAD is not an ideal Poisson model. Some parameters of the SPAD and the optics system are shown in Table 1.

When the dead time effect is taken into account, the actual probability mass function of y_k under fixed dead time and time-slot is [23]

$$P(y_k, \lambda_{s[k]}) \approx \frac{(\lambda_{s[k]}(1 - y_k\delta))^{y_k}}{y_k!} \exp(-\lambda_{s[k]}(1 - y_k\delta)) \tag{3}$$

Where $\lambda_{s[k]}$ is the average photons recieved by the SPAD, y_k is the photons output by the SPAD, $\delta = \tau / T_s$ is dead time ratio, and τ denotes the fixed dead time.

The model of time-slot synchronous clock extraction is established by considering the influences of communication rate, the number of gating signals and the number of photons in the time-slot on clock extraction. In our communication system, L_s is the synchronous character length, M is the number of gating signals, and $\Delta t = 2T_s/M$ is the offset of adjacent gating signalon the time axis. We assume that the time interval on the time axis is t, and the length of the character carrying the synchronization information is l. Therefore, the probability that the SPAD within t does not output photons can be expressed as

$$P(y_k = 0, l = 1, t) = \exp\left(-\lambda_{s[k]}\frac{t}{T_s}\right) \tag{4}$$

We assume that N_D is the photon count value in Δt. Then, the probability of adjacent gating signals with the same photon count value can be expressed as

$$P(y_k = N_D = 0, l = 1, \Delta t) = \exp\left(-\lambda_{s[k]}\frac{\Delta t}{T_s}\right) \tag{5}$$

In order to extract time-slot synchronization clock, the optimal gating signal corresponds to a count value that is greater than the count value corresponding to the others gating signals. We assume that the events of the detector output photons are independent of each other in different time-slot. The probability that the number of photons in adjacent gating signalis different can be expressed as

$$P(N_D = 1, 2, 3, \ldots, l = 1, \Delta t) = 1 - P(N_D = 0, l = 1, \Delta t) = 1 - \exp\left(-\lambda_{s[k]}\frac{\Delta t}{T_s}\right) \tag{6}$$

Therefore, the relation between the probability of successfully extracting time-slot synchronization clock and the required synchronous character length and the number of gating signals can be expressed as

$$P\left(N_D > 0, l = \frac{L_s}{2}, \Delta t\right) = 1 - \prod_{l=1}^{L_s/2} P\left(N_D = 0, l = \frac{L_s}{2}, \Delta t\right) = 1 - \left[\exp\left(-\frac{2\lambda_{s[k]}}{M}\right)\right]^{L_s/2} \tag{7}$$

It can be seen from Eq. (7) that when the number of gating signals is constant, the probability of successfully extracting the optimal time-slot synchronization clock is proportional to the length of the synchronous character and the number of photons in the time-slot.

2.3 Performance Estimation

We assume that n_1 is the photon counts of modulation signal output by the SPAD, and n_0 is the noise photon counts caused by the background light and dark count. According to the probability distribution of the photons output by the detector under the dead time limit, the maximum likelihood detection rule of symbol “1” and symbol “0” is [30]

$$\frac{P(y_k, \lambda_1)}{P(y_k, \lambda_0)} = \frac{\frac{(\lambda_1(1-y_k\delta))^{y_k}}{y_k!}\exp(-\lambda 1(1 - yk\delta))}{\frac{(\lambda_0(1-y_k\delta))^{y_k}}{y_k!}\exp(-\lambda_0(1 - y_k\delta))} \underset{\tilde{s}[k]=0}{\overset{\tilde{s}[k]=1}{\gtrless}} 1 \tag{8}$$

Where $\lambda_1 = n_1 + n_0$ represents the photon counts in time-slot “1” and $\lambda_0 = n_0$ represents the photon counts in time-slot “0”.

In the above model, the researcher considers that the photons in the time-slot are composed of noise photons and signal photons, and does not take into account that the synchronization error will cause the photon of time-slot “1” to be misjudged as belonging to time-slot “0”. In this paper, due to the photon detected by the randomness and synchronization error, the symbol deletion generated by the photon not detected in time-slot accounts for the majority, while the symbol error caused by background light and dark count is very few. The number of photons n_2 that are misjudged because

of synchronization error can be expressed as

$$n_2 = \frac{\Delta t}{2T_s}(n_1 + n_0) = \frac{n_1 + n_0}{M} \tag{9}$$

As can be seen from Eq. (7), when the number of photons in time-slot remains unchanged, the number of photons that are misjudged depends on the number of gating signals.

When the system transmits the symbol "1" and the symbol "0" with equal probability, the number of photons in a time-slot can be expressed as

$$\lambda_{s[k]} = \begin{cases} \lambda'_1 = n_1 + n_0 - n_2; \\ \lambda'_0 = n_0 + n_2; \end{cases} \tag{10}$$

Therefor, we rewrite Eq. (8) as

$$\frac{P(y_k, \lambda'_1)}{P(y_k, \lambda'_0)} = \frac{\frac{(\lambda'_1(1-y_k\delta))^{y_k}}{y_k!}\exp(-\lambda'_1(1-y_k\delta))}{\frac{(\lambda'_0(1-y_k\delta))^{y_k}}{y_k!}\exp(-\lambda'_0(1-y_k\delta))} \underset{\hat{s}[k]=0}{\overset{\hat{s}[k]=1}{\gtrless}} 1 \tag{11}$$

In this system, the bit error rate (BER) is derived from the misjudgment of the number of photons in time-slot. The probability that the time-slot "0" is misjudged as the symbol "1" is

$$\begin{aligned} P\{\hat{s}[k] = 1 | s[k] = 0\} &= P\{P\{y_k, \lambda'_1\} > P\{y_k, \lambda'_0\} | \lambda_{s[k]} = \lambda'_0\} \\ &= P\left\{y_k > \frac{\lambda'_1 - \lambda'_0}{\ln\lambda'_1 - \ln\lambda'_0} | \lambda_{s[k]} = \lambda'_0\right\} \\ &= \sum_{N=y_1}^{K_{\max}} \frac{(\lambda'_0(1-N\delta))^N}{N!}\exp(-\lambda'_0(1-N\delta)) \\ &= 1 - \sum_{N=0}^{y_1} \frac{(\lambda'_0(1-N\delta))^N}{N!}\exp(-\lambda'_0(1-N\delta)) \end{aligned} \tag{12}$$

Where $y1 = (\lambda'_1 - \lambda'_0)c/(\ln\lambda'_1 - \ln\lambda'_0)$. Similarly, the probability that time-slot "1" is misjudged as symbol "0" can be expressed as

$$P\{\hat{s}[k] = 0 | s[k] = 1\} = \sum_{N=0}^{y_1} \frac{(\lambda'_1(1-N\delta))^N}{N!}\exp(-\lambda'_1(1-N\delta)) \tag{13}$$

Therefore, the BER of system P_e can be expressed as

$$\begin{aligned} P_e &= \frac{1}{2}P\{\hat{s}[k] = 0 | s[k] = 1\} + \frac{1}{2}P\{\hat{s}[k] = 1 | s[k] = 0\} \\ &= \frac{1}{2}\left\{1 - \sum_{N=0}^{y_1}\left[\frac{(\lambda'_0(1-N\delta))^N}{N!}e^{-\lambda'_0(1-N\delta)} + \frac{(\lambda'_1(1-N\delta))^N}{N!}e^{-\lambda'_1(1-N\delta)}\right]\right\} \end{aligned} \tag{14}$$

3. Experiment Setup and Principle

The experimental setup of the photon-counting UOWC system is shown in Fig. 1. At the transmitting terminal, a field programmable gate array (FPGA) (Altera, DE-2) is used to convert the input data into non-return-to-zero on-off keying (NRZ-OOK) modulation signal, and the modulation signal is input to LED (CREE, Q5) drive circuit to drive LED output light wave signal. In order to simulate the long-distance and weak-link underwater communication environment, the diaphragm and many attenuators behind it are used to adjust the emitted light wave to the single photon state. The cylindrical water tank is 1.5 m in length and is filled with pure seawater. The focusing lens at the front of the water tank is used to expand field-of-view (FOV) so as to increase the received optical power. At last, the FPGA data processor performs clock and data recovery. We are committed to

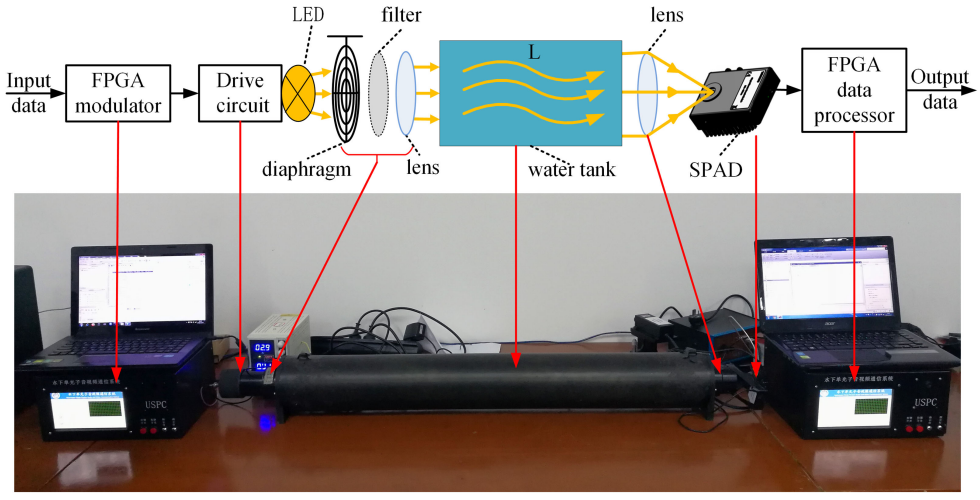

Fig. 1. Experimental setup of photon-counting UOWC.

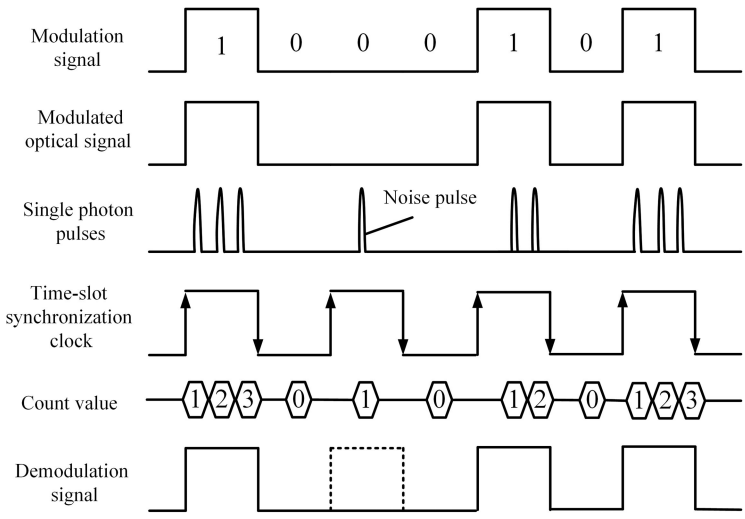

Fig. 2. The principle of photon-counting wireless optical communication.

verifying the method of extracting clock and data from single photon pulses. Due to the limited length of the water tank, longer distance communication is simulated by attenuating the power of the LED, the attenuation in the direction of communication is mainly caused by scattering and absorption. Since the communication rate is low and the communication distance is short, scattering is only considered as the cause of the attenuation. Other impact caused by scattering are very small and are therefore ignored.

The principle of photon-counting wireless optical communication is shown in Fig. 2. After the OOK modulated optical signal is attenuated by the channel, even if it becomes extremely weak when it arrives at the SPAD, the SPAD can still output discrete single photon pulses in some corresponding “1” time-slots. In addition, the number of single photon pulses in time-slot is random rather than fixed. There may be no single photon pulse (symbol deletion) in some time-slots corresponding to “1” due to fluctuations in photon flux and quantum efficiency of photon detection, and there may be noise pulse (symbol error caused by dark counts and background light) in some time-slots corresponding to “0”. However, as long as there are enough single photon pulses in the time-slots

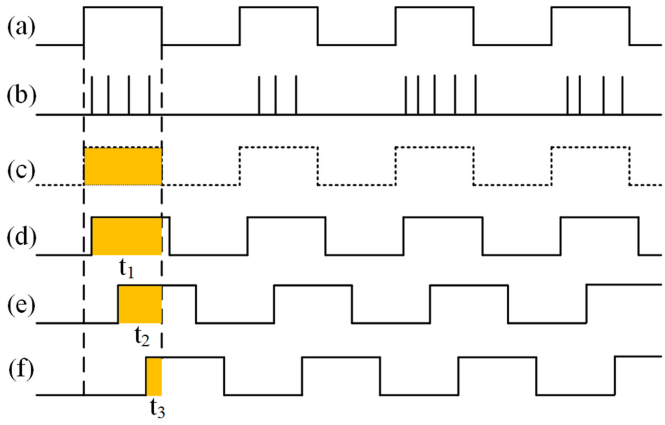

Fig. 3. The principle of time-slot synchronization clock recovery. (a) modualtion signal. (b) single photon pulse. (c) idle time-slot synchronization clock (d) gating signal 1. (e) gating signal 2. (f) gating signal 3.

corresponding to “1”, it can be considered that the communication system has a certain channel capacity. The signal demodulation method is to first recover the time-slot synchronization clock, and then count the single photon pulses in the time-slot synchronization clock. Finally, the time-slot is “1” when the count value is greater than the set threshold, and the time-slot is “0” when the count value is less than the set threshold.

4. The Method of Clock and Data Recovery

4.1 Time-Slot Synchronization Clock Recovery

The time-slot clock recovery method proposed in this paper is shown in Fig. 3. The transmitting terminal directly uses the time-slot synchronization clock as a modulated signal shown in (a), the detector outputs single photon pulses at the corresponding high level. In order to recover the clock in the receiving terminal, several clock signals with the same period and different phases is first generated. Moreover, phase is continuously incremented with p. If these clock signals act as gating signals to control a counter to count the single photon pulses output by the detector, count value after many period is proportional to the width of the overlapping portion of the high level (t_1, t_2, t_3). The maximum count value comes from the gating signals with the smallest phase difference from the time-slot clock, although it may not be apparent in a few periods due to fluctuations in photon flux and quantum efficiency of photon detection. Therefore, at the receiving terminal, we can select the gating signal corresponding to the maximum count value as the recovered clock signal.

The above time-slot synchronization clock recover method implemented on a FPGA is shown in Fig. 4, the circuit is composed of gating signal generator, counters, numeric comparator, signal selector, digital demodulator and control logic. Firstly, the gating signal generator is used to generate multiplex periodic square wave signals with the same width as time-slot synchronization clock. Meanwhile, the phase shift of each periodic square wave signal is the same. Then, these periodic square waves are input to the enable terminal of the corresponding counters. The arrived single photon pulse is counted within the high level of the periodic square wave signal, and the counter stops counting within the low level of the periodic square wave signal. After each count value is compared by the numeric comparator, the serial number of the counter with the maximum count value is sent to the signal selector. According to the serial number output by the numeric comparator, the signal selector outputs a gating signal as the recovered time-slot synchronization clock. Obviously, this time-slot synchronization clock recover method can be used for both OOK modulation and pulse position modulation (PPM) modulation.

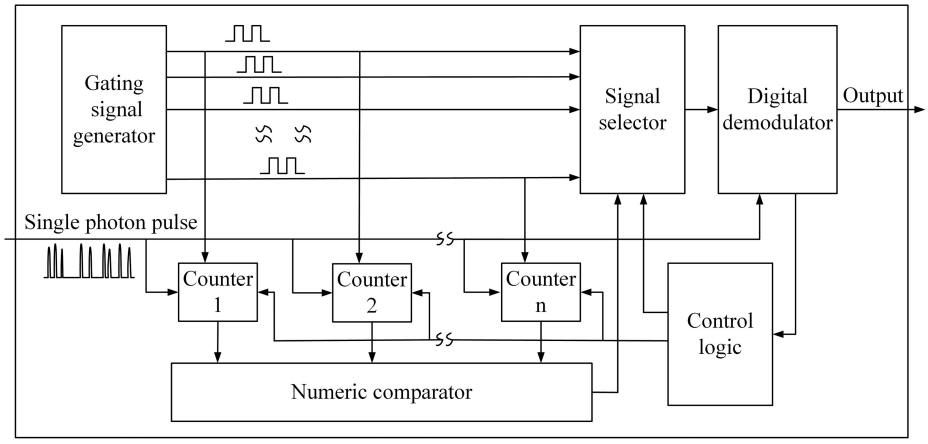

Fig. 4. The recovery circuit of the time-slot synchronization clock.

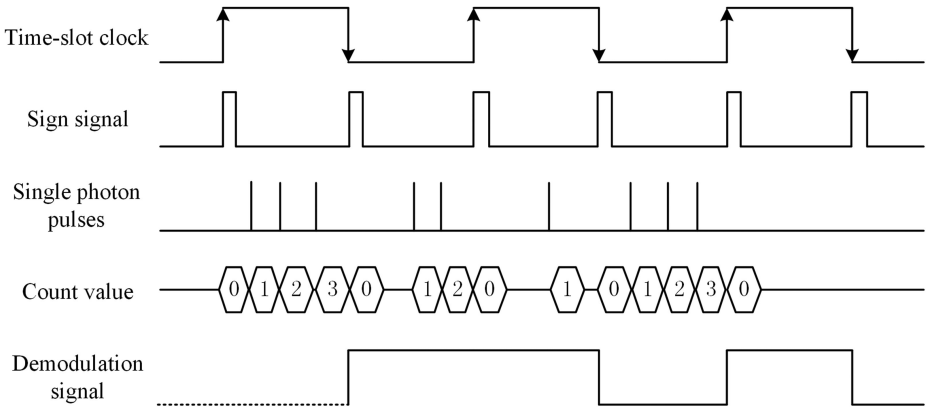

Fig. 5. The timing of signal demodulation.

4.2 Signal Demodulation Method Based on Photon-Counting

The data recovery method proposed in this paper is shown in Fig. 5. The digital demodulator based on FPGA includes edge detection, counter and decision device. The specific signal demodulation process is as follows. Firstly, when the edge detection detects the arrival of the rising edge and falling edge of time-slot clock, it outputs the sign signals to the counter. Then, after receiving the sign signals, the counter is cleared and starts to count the number of photons in time-slot clock. Finally, the decision device recoveries the data according to the relative value between the count value in time-slot and the threshold. As can be seen from Fig. 5, threshold is set to 2, when the number of photons in time-slot is greater than or equal to 2, the time-slot represents “1”, and when the number of photons the time-slot is less than 2, the time-slot represents “0”. In the experiment, the threshold is set based on the average number of photons and the average noise photons in the time-slot.

4.3 Frame Structure

According to the above analysis, the designed data frame structure is shown in Fig. 6. Bit sequence (0101 . . .) is used as synchronous character to generate time-slot synchronization clock. Besides, the length of synchronous character is not fixed and can be set according to the real-time requirements of the communication system. The frame header is a specific bit sequence (01111110),

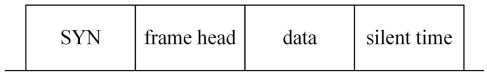

Fig. 6. Frame structure.

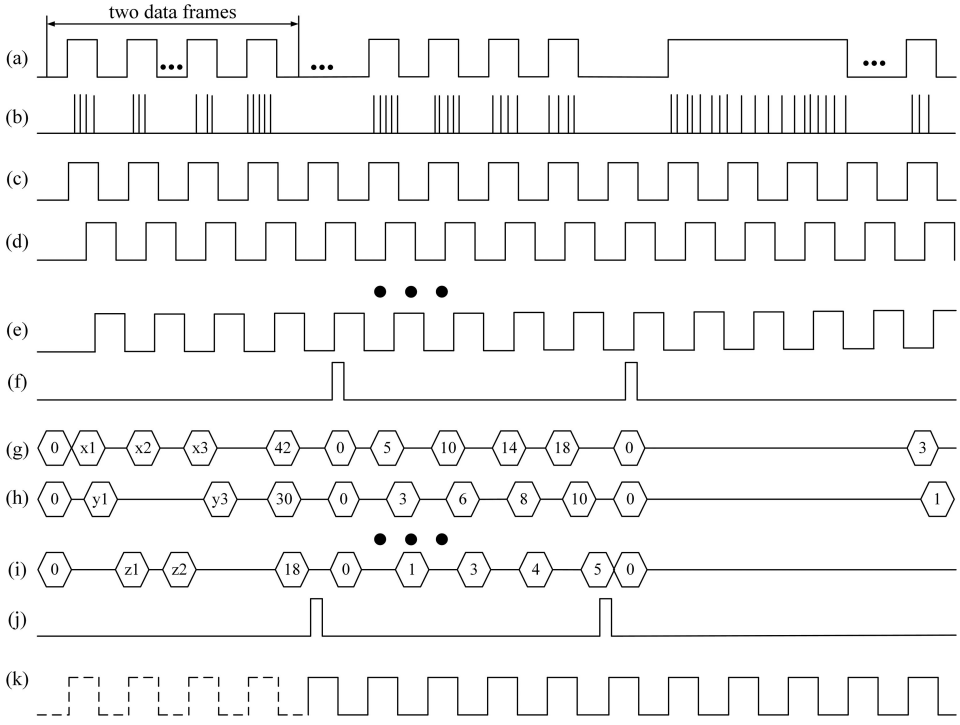

Fig. 7. The timing of clock and data recovery in our communication system. (a) modulation signal. (b) single photon pulse from SPAD. (c) gating signal 1. (d) gating signal 2. (e) gating signal Nth. (f) counter-reset signal. (g) count value 1. (h) count value 2. (i) count value Nth. (j) ouptut enable signal of signal selector. (k) time-slot synchronization clock.

which is utilized to perform frame synchronization and indicates the start and end of the frame. Behind the frame header is the 8-bit data to be transmitted, and the end of the frame is a silence period which does not transmit any information to distinguish adjacent data frames.

The timing of clock and data recovery in our communication system is shown in Fig. 7. After the system is reset, each counter is ready to receive single photon pulse sequences. Firstly, the counter counts the number of photons in the time scale of two data frames. Secondly, the signal selector selects the gating signal corresponding to the maximum count value as the time-slot synchronization clock. Finally, the demodulator recovers the time-slot information according to the time-slot synchronization clock, and performs the frame synchronization by detecting the frame head. When the next data frame arrives, the counter only needs to count the number of photons in synchronous character period, and time-slot synchronization clock extraction can be completed again. For OOK modulation, the time-slot synchronization clock is also the symbol synchronization signal.

5. Results and Discussion

5.1 Synchronous Character Length Versus BER

According to Eq. (7), with the increase of the synchronous character length l and the number of photons in time-slot, the probability of successfully extracting the optimal time-slot synchronization

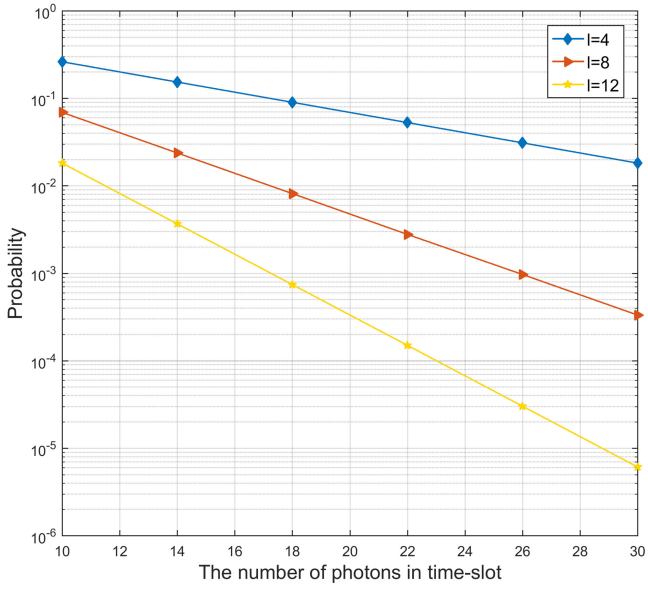

Fig. 8. The effect of synchronous character length on extracting time-slot synchronization clock.

clock increases. Fig. 8 shows the effect of the synchronous character length and the number of photons in time-slot on the results of extracting the optimal time-slot synchronization clock when the number of gating signals is $M = 30$. In Fig. 8, the ordinate indicates the failure probability to extract the optimal time-slot synchronization clock, and the abscissa indicates the average number of photons in the time-slot. Under the condition that the length of synchronous character is 4, 8, and 12 respectively, the failure probability of extracting the time-slot synchronization clock decreases as the average number of photons in the time-slot becomes larger. When the average number of photons in the time-slot is constant, the longer the synchronization character is, the lower the failure probability. As the average number of photons in the time-slot becomes larger, the gap of the probability failure consponding to different length of synchronous character also becomes larger.

Fig. 9 shows the relation between the synchronous character length and the average BER of the system when the communication rate is $R_b = 100$ Kbps and the number of gating signals is $M = 30$. It can be seen from the Fig. 9 that when the optimal demodulation threshold is selected, the BER of the system gradually decreases with the increase of the number of photons in time-slot and the synchronous character length. From the comparison between Fig. 8 and Fig. 9, it can be found that the synchronous characters length affects the probability of successful extraction of time-slot synchronization clock, and thus affects the performance of the system.

5.2 The Number of Gating Signals Versus BER

When the baud rate is constant, the number of gating signals determines the highest precision of time-slot synchronization clock. Fig. 10 shows the relation between the number of gating signals and the average BER of the system when the baud rate is $R_b = 100$ Kbps and the synchronization character length is $l = 12$. As can be seen from the Fig. 10, when the number of photons in time-slot is equal and the corresponding optimal demodulation threshold is selected, the system performance will be greatly improved as the number of gating signals increases from 10 to 15. This indicates that increasing the number of gating signals can improve the precision of the time-slot synchronization clock. Therefore, the average BER will be reduced. When the number of gating signals increases from 20 to 30, the average BER continues to decrease. However, the BER decreases little and the system performance tends to be stable. This indicates that although the system performance will

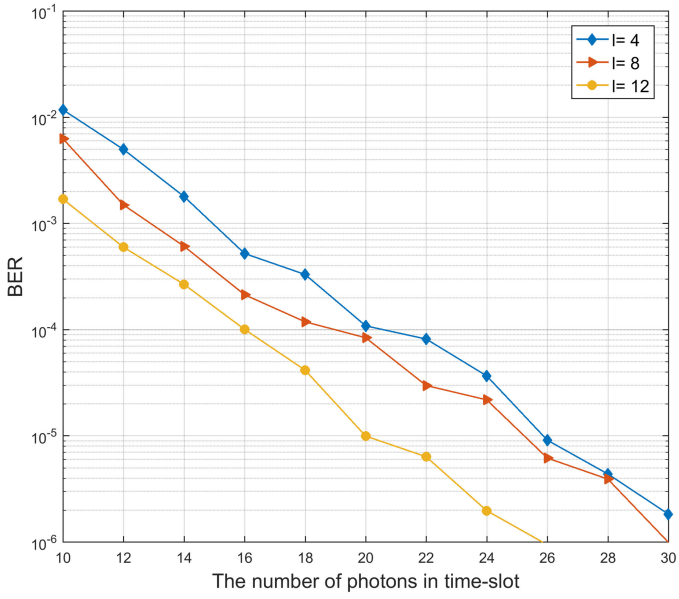

Fig. 9. BER performance with different synchronous character length.

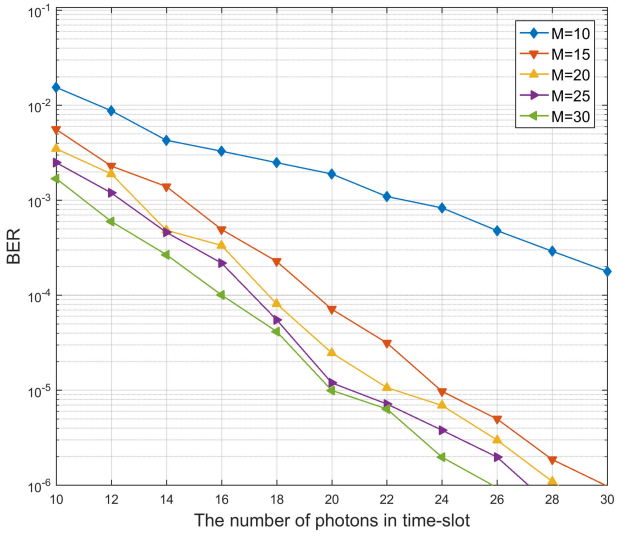

Fig. 10. BER performance with different number of gating signals.

be improved with the increase of the gating signals, the synchronization error has little effect on the performance of the system when the gating signal increases to a certain number.

5.3 The Baud Rate Versus BER

It can be seen from Eq. (3) that when the number of photons in time-slot is constant, the photons distribution output by the detector depends on the dead time ratio δ. The fixed dead time of the detector is $\tau = 40$, and the baud rate of the system determines the photons distribution. When the baud rate R_b are 1 Mbps, 500 Kbps, 200 Kbps, and 100 Kbps, the corresponding values δ are 0.04, 0.02, 0.008, and 0.004. Fig. 11 shows the probability distribution of the photons output by

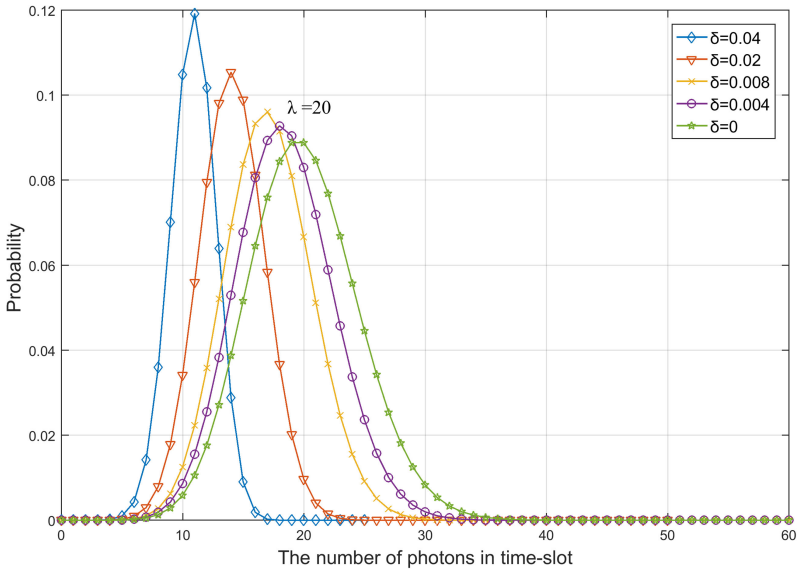

Fig. 11. The probability distribution for photons output by SPAD with dead time limit.

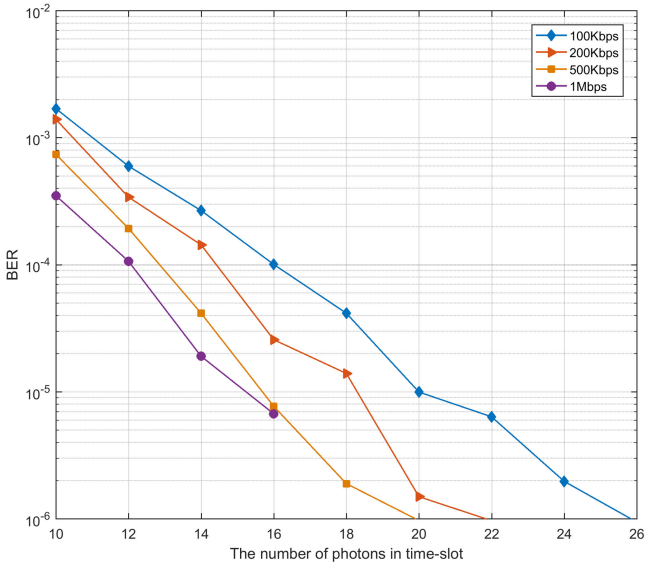

Fig. 12. BER performance with different baud rate.

the detector under different dead time ratio. It can be seen from Fig. 11 that as the dead time ratio increases, the sharper the probability distribution curve, the smaller the range of variation of the photon number in time-slot.

Fig. 12 shows the relation between baud rate and BER. It can be seen from the Fig. 12 that as the number of photons in time-slot increases, the BER gradually decreases. When the number of photons in time-slot is equal, the higher baud rate, the lower BER. When the BER is lower than 10^{-6} and the data rate is 100 Kbps, 200 Kbps, and 500 Kbps, the number of photons in time-slot is 26, 22, and 20, respectively. In Ref. [39], the photon number of each symbol is less than 100 and the BER is greater than 10^{-3}. It can be seen from Fig. 12 that the photon-counting UOWC with a BER of 3.51×10^{-4} and a baud rate of 1 Mbps can be achieved by using 10 photons in the time-slot.

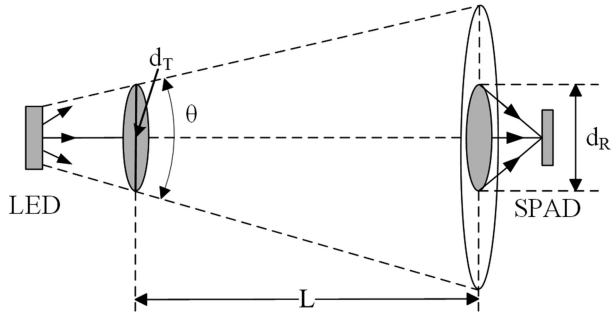

Fig. 13. The schematic diagram of optical signal propagation.

TABLE 2
The Parameters of the Two Waters Quality

water quality	a(λ)(m^{-1})	b(λ)(m^{-1})
Pure Seawater (I)	0.053	0.003
Clean Ocean (II)	0.069	0.08

5.4. Theoretical Communication Distance

The propagation model of the optical signal is shown in the Fig. 13. The attenuation caused by divergence of optical signals, scattering and absorption in underwater channels are considered to calculate the theoretical communication distance. The divergence angle θ of collimator is equal to 0.1°. The diameter of transmitting end d_T and the diameter of receiving end d_R are equal to 6cm. The attenuation coefficient by the divergence of the optical signal in the propagation process can be expressed as

$$\varepsilon_{div} = \left(\frac{d_R}{d_T + L * \theta}\right)^2 \tag{15}$$

According to Beer Law, the attenuation caused by scattering and absorption in underwater channels can be expressed as [36], [37]

$$\varepsilon_{water} = e^{-[a(\lambda)+b(\lambda)]L} \tag{16}$$

Where $a(\lambda)$ denotes the absorption coefficient, $b(\lambda)$ denotes scattering coefficient. The attenuation coefficient of pure seawater and clear seawater are shown in the Table 2 [38]. Therefore, the cumulative attenuation in our proposed system is expressed as follow

$$p_R = p_T * e^{-[a(\lambda)+b(\lambda)]L} \left(\frac{d_R}{d_T + L * \theta}\right)^2 \tag{17}$$

Where p_T denotes the optical power at the transmitting terminal, p_R denotes the optical power at the receiving terminal.

Optical power at the receiving terminal corresponding to the number of photons in a time-slot can be expresed as

$$p_R = \frac{Nhv}{tC_{PDE}} \tag{18}$$

Where N denotes the photon number in a time-slot, h denotes the Planck constant, v denotes the optical frequency, t denotes the the width of time-slot, C_{PDE} is the quantum efficiency of SPAD. For

TABLE 3
Theoretical Communication Distance

Photons	Baud rate	p_R	water quality	Distance	BER
10	1 Mbps	-79.45 dBm	I/II	362m/144m	$<10^{-3}$
10	500 Kbps	-82.46 dBm	I/II	373m/150m	$<10^{-3}$
20	200 Kbps	-82.43 dBm	I/II	373m/150m	$<10^{-5}$
20	100 Kbps	-86.44 dBm	I/II	389m/154m	$<10^{-4}$

example, using the clock and data recovery methods proposed in this paper, when the Baud rate is 1Mbps and average 10 photons in one time-slot, a BER of less than 10^{-3} can be achieved. At this time the corresponding optical power p_R is -79.45 dBm. In Ref. [40], when the communication rate is 5 MHZ, the optical power of the receiver is -62.8 dBm. If we adopt the communication rate of 5 MHz, even if the optical power of the receiver will increase to -72.46 dBm, it is still below -62.8 dBm. According to Eq. (17) and Eq. (18), when p_T is set to 30 dBm (1W), the communication distance under in pure seawater can be calculated to be 362 m. The theoretical communication distances for other parameters can also be found in Table 3.

6. Conclusion

An experimental system for simulating long-distance photon-counting UOWC is built. On this basis, a method of directly recovering clock and data from discrete random pulse sequence output by the SPAD is proposed and implemented. A new communication model is established, taking into account not only fluctuations in photon flux and quantum efficiency of photon detection in a time-slot, but also the phase difference of the recovered clock caused by it. The effects of the system setting parameters such as the number of gate signals, synchronous character length and baud rate on the average BER were verified by experiments. The experimental results show that increasing the number of photons in time-slot and the length of synchronous characters is beneficial to recovering time-slot synchronization clock, thus reducing the BER of system. Under the same experimental conditions, the more the number of gating signals, the higher the precision of the time-slot synchronization clock, and the better the system performance. The variation range of photons in time-slot decreases with the increase of baud rate, which leads to the reduction of BER. When the number of gating signals is set to 30, the length of synchronous characters is set to 12 and the baud rate is set to 1 Mbps, photon-counting UOWC with and a BER of 3.51×10^{-4} can be achieved under condition of only average 10 photons in one time-slot. If 256-PPM is used instead of OOK, then one time-slot can represent 8 bits and eventually 1.25 photons/bit can be achieved.

References

[1] Z. Zeng, S. Fu, H. Zhang, Y. Dong, and J. Cheng, "A survey of underwater optical wireless communications," *IEEE Commun. Surv. Tut.*, vol. 19, no. 1, pp. 204–238, Jan.–Mar. 2017.
[2] S. Arnon, "Underwater optical wireless communication network," *Opt. Eng.*, vol. 49, 2010, Art. no. 015001.
[3] L. Lanbo, Z. Shengli, and C. Jun-Hong, "Prospects and problems of wireless communication for underwater sensor networks," *Wireless Commun. Mobile Comput.*, vol. 8, pp. 977–994, 2008.
[4] H. Kaushal and G. Kaddoum, "Underwater optical wireless communication," *IEEE Access*, vol. 4, pp. 1518–1547, 2016.
[5] H. M. Oubei *et al.*, "4.8 Gbit/s 16-QAM-OFDM transmission based on compact 450-nm laser for underwater wireless optical communication," *Opt. Exp.*, vol. 23, pp. 23302–23309, 2015.
[6] H. M. Oubei, C. Li, K.-H. Park, T. K. Ng, M.-S. Alouini, and B. S. Ooi, "2.3 Gbit/s underwater wireless optical communications using directly modulated 520 nm laser diode," *Opt. Exp.*, vol. 23, pp. 20743–20748, 2015.
[7] C. Wang, H.-Y. Yu, Y.-J. Zhu, T. Wang, and Y.-W. Ji, "Multi-LED parallel transmission for long distance underwater VLC system with one SPAD receiver," *Opt. Commun.*, vol. 410, pp. 889–895, 2018.

[8] X. Liu *et al.*, "34.5 m underwater optical wireless communication with 2.70 Gbps data rate based on a green laser diode with NRZ-OOK modulation," *Opt. Exp.*, vol. 25, pp. 27937–27947, 2017.
[9] P. Wang, C. Li, and Z. Xu, "A cost-efficient real-time 25 Mb/s system for LED-UOWC: Design, channel coding, FPGA implementation, and characterization," *J. Lightw. Technol.*, vol. 36, no. 13, pp. 2627–2637, Jul. 2018.
[10] C. Wang, H.-Y. Yu, Y.-J. Zhu, and T. Wang, "Blind detection for SPAD-based underwater VLC system under P–G mixed noise model," *IEEE Commun. Lett.*, vol. 21, no. 12, pp. 2602–2605, Dec. 2017.
[11] K. Nakamura, I. Mizukoshi, and M. Hanawa, "Optical wireless transmission of 405 nm, 1.45 Gbit/s optical IM/DD-OFDM signals through a 4.8 m underwater channel," *Opt. Exp.*, vol. 23, pp. 1558–1566, 2015.
[12] H. Uema, T. Matsumura, S. Saito, and Y. Murata, "Research and development on underwater visible light communication systems," *Electron. Commun. Jpn.*, vol. 98, pp. 9–13, 2015.
[13] P. Tian *et al.*, "High-speed underwater optical wireless communication using a blue GaN-based micro-LED," *Opt. Exp.*, vol. 25, pp. 1193–1201, 2017.
[14] W.-Y. Lin *et al.*, "10m/500Mbps WDM visible light communication systems," *Opt. Exp.*, vol. 20, pp. 9919–9924, 2012.
[15] C.-W. Chow, R.-J. Shiu, Y.-C. Liu, Y. Liu, and C.-H. Yeh, "Non-flickering 100 m RGB visible light communication transmission based on a CMOS image sensor," *Opt. Exp.*, vol. 26, pp. 7079–7084, 2018.
[16] Z. Ghassemlooy, S. Arnon, M. Uysal, Z. Xu, and J. Cheng, "Emerging optical wireless communications-advances and challenges," *IEEE J. Sel. Areas Commun.*, vol. 33, no. 9, pp. 1738–1749, Sep. 2015.
[17] X. Huang, Z. Wang, J. Shi, Y. Wang, and N. Chi, "1.6 Gbit/s phosphorescent white LED based VLC transmission using a cascaded pre-equalization circuit and a differential outputs PIN receiver," *Opt. Exp.*, vol. 23, pp. 22034–22042, 2015.
[18] A. Jovicic, J. Li, and T. Richardson, "Visible light communication: opportunities, challenges and the path to market," *IEEE Commun. Mag.*, vol. 51, no. 12, pp. 26–32, Dec. 2013.
[19] C.-H. Yeh, Y.-L. Liu, and C.-W. Chow, "Real-time white-light phosphor-LED visible light communication (VLC) with compact size," *Opt. Exp.*, vol. 21, pp. 26192–26197, 2013.
[20] C.-H. Yeh, B.-S. Guo, Y.-J. Chang, C.-W. Chow, and C.-S. Gu, "Bidirectional free space optical communication (FSO) in WDM access network with 1000-m supportable free space link," *Opt. Commun.*, vol. 435, pp. 394–398, 2019.
[21] S. Hu, L. Mi, T. Zhou, and W. Chen, "35.88 attenuation lengths and 3.32 bits/photon underwater optical wireless communication based on photon-counting receiver with 256-PPM," *Opt. Exp.*, vol. 26, pp. 21685–21699, 2018.
[22] C. Wang, H.-Y. Yu, and Y.-J. Zhu, "A long distance underwater visible light communication system with single photon avalanche diode," *IEEE Photon. J.*, vol. 8, no. 5, Oct. 2016, Art. no. 7906311.
[23] C. Wang, H.-Y. Yu, Y.-J. Zhu, T. Wang, and Y.-W. Ji, "Experimental study on SPAD-based VLC systems with an LED status indicator," *Opt. Exp.*, vol. 25, pp. 28783–28793, 2017.
[24] T. Shafique, O. Amin, M. Abdallah, I. S. Ansari, M.-S. Alouini, and K. Qaraqe, "Performance analysis of single-photon avalanche diode underwater VLC system using ARQ," *IEEE Photon. J.*, vol. 9, no. 5, Oct. 2017, Art. no. 7906313.
[25] P. A. Hiskett, R. A. Struthers, R. Tatton, and R. Lamb, "A photon-counting optical communication system for underwater data transfer," *Proc. SPIE*, vol. 8542, 2012, Art. no. 854214.
[26] T. Mao, Z. Wang, and Q. Wang, "Receiver design for SPAD-based VLC systems under Poisson–Gaussian mixed noise model," *Opt. Exp.*, vol. 25, pp. 799–809, 2017.
[27] M.-A. Khalighi, T. Hamza, S. Bourennane, P. Léon, and J. Opderbecke, "Underwater wireless optical communications using silicon photo-multipliers," *IEEE Photon. J.*, vol. 9, no. 4, Aug. 2017, Art. no. 7905310.
[28] T. Hamza, M.-A. Khalighi, S. Bourennane, P. Leon, and J. Opderbecke, "On the suitability of employing silicon photo-multipliers for underwater wireless optical communication links," in *Proc. 10th Int. Symp. Commun. Syst., Netw. Digital Signal Process.*, 2016, pp. 1–5.
[29] F. Bellei *et al.*, "Free-space-coupled superconducting nanowire single-photon detectors for infrared optical communications," *Opt. Exp.*, vol. 24, pp. 3248–3257, 2016.
[30] Y.-W. Ji, G.-F. Wu, C. Wang, and E.-F. Zhang, "Experimental study of SPAD-based long distance outdoor VLC systems," *Opt. Commun.*, vol. 424, pp. 7–12, 2018.
[31] C. Wang, H. Yu, Y.-J. Zhu, T. Wang, and Y. Ji, "One symbol training receiver for the SPAD-based UVLC system," *Appl. Opt.*, vol. 57, pp. 5852–5858, 2018.
[32] Y. Xia-Chao *et al.*, "Model of bit error rate for laser communication based on superconducting nanowire single photon detector," *Acta Phys. Sinica*, vol. 66, 2017.
[33] Y.-D. Zang, J. Zhang, and L.-H. Si-Ma, "Anscombe root DCO-OFDM for SPAD-based visible light communication," *IEEE Photon. J.*, vol. 10, no. 2, Apr. 2018, Art. no. 7902509.
[34] P. A. Hiskett and R. A. Lamb, "Underwater optical communications with a single photon-counting system," in *Proc. SPIE*, vol. 9114, 2014, Art. no. 91140P.
[35] J. Shen *et al.*, "Towards power-efficient long-reach underwater wireless optical communication using a multi-pixel photon counter," *Opt. Exp.*, vol. 26, pp. 23565–23571, 2018.
[36] Y. Xiang, L. Zan, and L. Zengji, "Underwater optical communication performance for laser beam propagation through weak oceanic turbulence," *Appl. Opt.*, vol. 54, pp. 1273–8, 2015.
[37] J. B. Snow *et al.*, "Underwater propagation of high-data-rate laser communications pulses," *Proc. SPIE*, vol. 1750, pp. 419–427, 1992.
[38] T. J. Petzold, "Volume scattering functions for selected ocean waters," Scripps Institution of Oceanography La Jolla Ca Visibility Lab, University of California, San Diego, CA, USA, 1972.
[39] J. Shen *et al.*, "Single LED-based 46-m underwater wireless optical communication enabled by a multi-pixel photon counter with digital output," *Opt. Commun.*, vol. 438, pp. 78–82, 2019.
[40] J. Shen *et al.*, "Towards power-efficient long-reach underwater wireless optical communication using a multi-pixel photon counter," *Opt. Exp.*, vol. 26, pp. 23565–23571, 2018.